Energy Reports 7 (2021) 7693–7703

Contents lists available at ScienceDirect

Energy Reports

journal homepage: www.elsevier.com/locate/egyr

Research paper

Experimental investigation of a loop heat pipe with a flat evaporator and cupric oxide nanofluids as working fluid

Tianyuan Zhao [a], Zhengyuan Ma [a], Zikang Zhang [a], Weizhong Deng [a], Rui Long [a], Wei Liu [a], Lei Ma [b,*], Zhichun Liu [a,*]

[a] School of energy and power engineering, Huazhong University of Science and Technology, Wuhan, 430074, China
[b] Coll New Mat & New Energies, Shenzhen Technol Univ, Shenzhen 518118, China

ARTICLE INFO

Article history:
Received 27 August 2021
Received in revised form 25 October 2021
Accepted 31 October 2021
Available online 22 November 2021

Keywords:
Loop heat pipe
Flat evaporator
Nanofluids
Heat transfer enhancement

ABSTRACT

Loop heat pipe (LHP) is widely used in high-power electronic cooling as a passive cooling device. In this paper, the LHP system was designed with a flat evaporator and a capillary biporous wick with cupric oxide nanofluids as working fluid in LHP. The capillary biporous wick was sintered by nickel powder and the nanofluids were prepared by a two-step method. The startup tests, variable heat load tests, and performance degradation tests of LHP were conducted respectively and the thermal resistance was further analyzed. The results showed that, compared with distilled water, the maximum heat load increased from 290 W to 310 W and the minimum startup heat load decreased from 40 W to 20 W with nanofluids as working fluid. Both the temperature of the evaporator wall and the thermal resistance were reduced in startup tests. At the heat load of 50 W, the performance improvement was the most noticeable, where the temperature of the evaporator wall was reduced by 12.7 °C, the thermal resistance of the evaporator was reduced by 26.9%, and the thermal resistance of the LHP system was reduced by 17.6%. With a variable heat load ranging from 50 W to 290 W, the response speed of LHP became faster and the temperature fluctuation was smaller. The LHP with nanofluids as working fluid still operated normally and the change of thermal resistance with the varies of heat load had the same tendency as the previous experiment in performance degradation tests of 2 months.

© 2021 The Authors. Published by Elsevier Ltd. This is an open access article under the CC BY-NC-ND license (http://creativecommons.org/licenses/by-nc-nd/4.0/).

1. Introduction

In aerospace thermal management, the condition of electronics cooling is so strict that the traditional single-phase cooling method assisted with pumps has no longer fulfilled the requirement of power consumption, quality, and reliability in space. Loop heat pipe (LHP) is a kind of two-phase heat transfer device based on capillary driving, which can remove large heat in a long distance with a small temperature difference (Maydanik, 2005). Based on these advantages, LHP seems to be applied widely in aerospace cooling in the future (Wang et al., 2014).

The thermophysical properties of working fluid in LHP such as thermal conductivity, latent heat of vaporization, and boiling point are the important factors of limitation in the thermal appearance of LHP. The common working fluids in LHP such as water, methanol, and ammonia have different limitations in latent heat of vaporization, boiling point, toxicity, and material compatibility. The thermal conductivity of working fluid has a great influence on the thermal appearance of LHP, which may not cause operation failure but is related to the heat transfer efficiency of LHP. In 1995, Choi et al. put forward the concept of nanofluids: one kind of new heat transfer medium that metal or non-metal nanoparticles are dispersed and suspended uniformly and stably in traditional heat transfer medium, which has been applied in the field of heat transfer enhancement by researchers (Choi, 1995). Choi and Eastman et al. respectively tested the thermal conductivity of several nanofluids such as Al_2O_3-water, SiO_2-water, TiO_2-water, and the thermal conductivity of CuO-water nanofluids with volume fraction less than 5% increased by 15% compared with that of distilled water (Choi et al., 1999).

Since nanofluids have higher thermal conductivity than traditional working fluids, some researchers have begun to apply them in heat pipes as working fluids. The application of the nanofluids in heat pipes is still in the initial process, most of which are experimental. In these researches, the type of heat pipes, the geometry size, the base fluid, the variety of and nanoparticles are quite different. The nanoparticles used in nanofluids include metals, metal oxides, carbon nanotubes, and graphene commonly. The types of heat pipes involved include traditional heat pipes, oscillating heat pipes (OHP), loop heat pipes (LHP), etc.

There are many experimental studies on traditional heat pipes and pulsating heat pipes with nanofluids as working fluids.

* Corresponding authors.
E-mail addresses: malei@sztu.edu.cn (L. Ma), zcliu@hust.edu.cn (Z. Liu).

https://doi.org/10.1016/j.egyr.2021.10.114
2352-4847/© 2021 The Authors. Published by Elsevier Ltd. This is an open access article under the CC BY-NC-ND license (http://creativecommons.org/licenses/by-nc-nd/4.0/).

Nomenclature

ID	Inter diameter [mm]
M	Mass [kg]
OD	Outer diameter [mm]
R	Thermal resistance [°C/W]
T	Temperature [°C]
V	Internal volume [m^3]
Q	Heat load [W]

Greek symbol

α	Charging ratio
β	Vapor-phase share in the compensation chamber
ω	Mass concentration of nanoparticle
ε	Porosity

Subscripts

base	Base fluid
cc	Compensation chamber
cond	Condensation
eva	Evaporator
ll	Liquid line
total	Total system
wick	Capillary wick

Abbreviations

eva_out	Evaporator outlet
LHP	Loop heat pipe
SDBS	Sodium dodecyl benzene sulfonate
TC	Thermocouple

In 2004, Chen et al. used gold-water nanofluids in a conventional heat pipe which was the first time that the nanofluids were adopted in heat pipe (Tsai et al., 2004). The heat pipe had a length of 170 mm and an outer diameter of 6 mm and its thermal resistance with nanofluids was lower than heat pipe with distilled water. Zaaroura et al. conducted experiments on the impact of gold-water nanofluids with a diameter of 5 nm on improving the characteristics of heat transfer in a capillary heat pipe (Zaaroura et al., 2021), the results showed the positive influence of gold-water nanofluids on the heat pipe by reducing the thermal resistance of system by 13% compared to distilled water as working fluid. Sözen et al. conducted an experiment on the heat pipe with aqueous clinoptilolite nanofluid specifically in higher heating loads, which maximum heat transfer enhancement and the improvement in thermal resistance of the heat pipe were obtained as 9.63% and 26.31%, respectively (Sözen et al., 2019). Martin et al. executed an experimental work with a hybrid nanofluid that involves Fe and CuO nanoparticles prepared by the two-step method and then tested in a plain heat pipe., which average wall temperature differences between the evaporator and the condenser regions, heat pipe's thermal resistance, and efficiency all performed better than distilled water (Martin et al., 2020). Aydin et al. set up an experimental test rig to test two different nanofluids each of which involves different base fluid, concentration, and surfactant type (Yilmaz Aydin et al., 2021a; Yılmaz Aydın et al., 2021b). Sözen et al. investigated how TiO2/distilled water nanofluids influence the thermal performance of a two-phase closed thermosiphon at various states of operation and used different surfactants (Triton X-100 and sodium dodecylbenzene sulfonate surfactants) to prepare for the nanofluids (Sözen et al., 2018b,a). Gürü et al. experimented to investigate the influences of bentonite-deionized water nanofluid utilization at different concentrations on heat pipe performance and the best nanoparticle concentration of nanofluids was 2% in terms of thermal performance and cost (Gürü et al., 2019). Liu et al. studied the CuO-water nanofluids effect in the startup process and steady operation of a cylindrical miniature grooved heat pipe, the results showed that in the startup process, nanofluids reduced the response time of the heat pipe and maximum heat transfer capacity of the heat pipe increased by 40% (Wang et al., 2010). Riehl et al. conducted experiments on an open-loop pulsating heat pipe with water and copper–water nanofluid, which showed better performance at higher heat loads with nanofluids (Riehl and Santos, 2012). Zhou et al. designed a cylindrical miniature heat pipe and tests showed that nanofluids had a slightly slower startup response compared to distilled water while the maximum heat transfer capability with nanofluids was greatly promoted (Zhou et al., 2019). There are also some simulation studies about nanofluid in heat pipes. Sadeghinezhad et al. investigated the thermal performance of conventional sintered heat pipe with graphene nanofluid and it was found that 0.1 wt% concentration of nanofluid exhibited the best heat transfer performance (Sadeghinezhad et al., 2016). Most of the studies show that nanofluids were beneficial to heat pipe heat transfer performance, but there are few studies on loop heat pipe of the nanofluid working fluid. Wan et al. used Cu–water nanofluids as working fluid in a miniature loop heat pipe and the nanofluids were composed of distilled water and Cu nanoparticles with an average diameter of 50 nm. It was found that the evaporator wall and thermal resistance of the system were reduced by 12.8% and 21.7%, respectively, and the optimal mass concentration of the nanofluids for maximum heat transfer coefficient was 1.5 wt% (Wan et al., 2015). Liu et al. carried out an experiment of a loop heat pipe with Cu–water nanofluids as working fluid, which was composed of distilled water and copper oxide nanoparticles with an average diameter of 50 nm. The experimental results showed that, compared with distilled water, the heat transfer coefficient of the loop heat pipe at the optimal mass concentration (1.0 wt%) was 45% higher under stable conditions, the maximum heat flux was 20% higher, the startup time was 20% lower, and the evaporator wall temperature was 2 °C lower, but the maximum startup heat load could not be improved (Li et al., 2010). Trijo et al. tested the thermal performance of a micro loop heat pipe with graphene-water that the thickness of the graphene nanoparticles was 1−5 nm and entropy generation analysis of the micro loop heat pipe was conducted (Tharayil et al., 2017, 2016). The experimental results showed that at the heat load ranging from 20–380 W, with the increase of concentration of nanofluids, the temperature difference between evaporator and the condenser and thermal resistance was reduced, and the heat transfer coefficient of LHP, effective thermal conductivity and thermal efficiency increased, respectively. And the use of nanofluids diminished the entropy generation of the micro loop heat pipe that could reduce by 34.6% most significantly. Putra et al. applied Al_2O_3-water nanofluids to the loop heat pipe, and the capillary wick was sintered with biological materials (Putra et al., 2014). The experimental results showed that the optimal mass fraction of the nanofluids in the experiment was 1%, and the thermal resistance of all cases with 1%, 3% and 5% Al_2O_3-water nanofluids in loop heat pipes was lower than that of distilled water. Most of these experimental results showed that the nanofluids as working fluid in LHP increased the maximum heat flux, decreased the system thermal resistance/startup time, and increased the heat transfer coefficient. The explanations for improving the thermal performance of LHP include that the thermal conductivity increased, contact angle decreased, and the amount of vaporization at the

evaporation surface was increased and the Brownian motion of nanoparticles resulted in an increased "convection" effect (Alawi et al., 2014; Gupta et al., 2018; Liu and Li, 2012).

It can be noted from the above literature review that: the nanofluids have never been used as working fluid in a sintered capillary wick in LHPs, the wire mesh wicks were adopted in most researches, the pore diameter was large and the capillary force was insufficient. The capillary wick sintered by metal with a smaller pore diameter might be more suitable for the LHP, which was also the motivation for conducting this experiment. Some studies about capillary wick in LHP showed that biporous wick was suitable for LHP system with long heat transfer distance since it showed higher thermal performance than conventional wick (Ji et al., 2017; Nakamura et al., 2016; Semenic et al., 2008). A biporous wick has a structure with bimodal pore size distribution. For the fabrication method introduced in Ref. Chen et al. (2012), Yeh et al. (2009) and Zhao et al. (2021), small pores could be formed by sintering metal powder, and large pores could be formed by dissolving the pore formers of sodium carbonate (Na_2CO_3). The most distinctive advantage of biporous wick is two different pore distributions that large pores can reduce the flow resistance while small pores can maintain high capillary force.

In this study, CuO–H2O nanofluids with a mass fraction of 0.5%wt were used in a flat evaporator with a nickel powder sintered capillary biporous wick. According to the above literature review, nanofluids have not been applied in a capillary biporous wick before. The capillary biporous wick sintered by nickel powder with high porosity of 71% and a small pore diameter of fewer than 50 μm was adopted in the LHP, and a flat evaporator which was easier to fit the heating wall was set up in the system. The startup tests, variable heat load tests, and performance degradation tests of LHP were conducted respectively and the thermal resistance was analyzed to test heat transfer performance of the designed LHP system with nanofluids as working fluid and to compare with distilled water.

2. Experimentation

2.1. Description of LHP

The system of LHP consists of four parts that evaporator, condenser, liquid line, and vapor line. Traditional evaporators are commonly cylindrical. However, existing studies suggest that the angle between the flow velocity direction of working fluid and the temperature gradient in a flat evaporator is smaller than that in a cylindrical evaporator, which can reduce the heat resistance of the evaporator (Liu et al., 2007). There was a compensation chamber (CC) and a capillary biporous wick sintered by metal powders integrated with the circular flat evaporator. The height of the flat evaporator was 18.5 mm and the capillary wick was sintered by nickel powders under the instructions in Ref. Li et al. (2012). In this study, the sinter powders were T255 nickel powders with a particle size of 2.2–2.8 μm and $NaCO_3$(sodium carbonate) powders with particle sizes ranging from 50-75 μm were chosen as the pore former, which are same in Ref. He et al. (2018) and Zhang et al. (2021). The porosity of the wick was tested at about 71% and the pore diameters were less than 50 μm. A tube-in-tube condenser was used for cooling in this system. The cooling water system was a constant temperature tank, and the refrigerant water was a 50% glycol aqueous solution. The lowest water temperature could be provided was −20 °C. Both the vapor line and liquid line were made of copper pipes with an internal/external diameter of 4/6 mm. The evaporator and the condenser were arranged at the same height on an optical bench so that the tilt angle was 0°. The specifications of LHP are presented in Table 1. The internal structure is shown in Fig. 1 and the appearance of the capillary wick is shown in Fig. 2. The schematic diagram of the LHP shows in Fig. 3.

Table 1
Parameters of the LHP.

Component	Dimensions	Value
Evaporator	Overall height (mm)	18.5
	Heated diameter (mm)	36
	OD (mm)	80
Compensation chamber	Height (mm)	10.5
	OD (mm)	34.5
Capillary wick	Thickness (mm)	2.2
	OD (mm)	37.3
	Porosity (%)	71
Vapor line	OD/ID (mm)	6/4
	Length (mm)	375
Liquid line	OD/ID (mm)	6/4
	Length (mm)	220
Condensation	OD (mm) for working fluid	6
	OD (mm) for the coolant	12
	Length(mm)	650
Tilt angle	Angle (°)	0

Table 2
Locations of thermocouples.

Locations	TC number
Heat source	TC1–TC4
Upper evaporator	TC5
Compensation chamber	TC6
Evaporator outlet	TC7
Vapor line	TC8
Condenser inlet	TC9
Condenser outlet	TC10
Liquid line	TC11
Evaporator outlet	TC12
Ambient	TC13

The charging ratio of working fluid was 65%, which is determined by the following two equations (Ku, 2007):

$$\alpha V_{total} \geq V_{cond} + V_{ll} + \varepsilon V_{wick} + (1-\beta) V_{cc} \quad (1)$$

$$\alpha V_{total} < V_{cond} + V_{ll} + \varepsilon V_{wick} + V_{cc} \quad (2)$$

where α denotes the charging ratio, V_{total}, V_{cond}, V_{ll}, V_{wick} and V_{cc} denote the internal volume of the total system, condenser, liquid line, wick, and compensation chamber, respectively, and ε denotes the porosity of capillary wick and β denotes vapor phase share in the compensation chamber whose value is 0.5 in the equation (Singh et al., 2008). The system was vacuumed to 3.4×10^{-4} Pa for reducing the influence of non-condensable gas. A red copper cylinder with a diameter of 36 mm was used for the simulated heat source, inserted with three heating rods and was wrapped with insulation material (a rubber sponge, thermal conductivity 0.04 W/m K) to avoid heat loss to the environment, and the power was changed by adjusting the voltage regulator to realize different thermal loads and measured by a power meter with 0.5% accuracy. The data acquisition system adopted t-type thermocouples TC_1-TC_{13} to obtain the temperature of each point in the system. The error of thermocouple was ±0.5 °C after calibration of linear compensation in a water bath ranging from 10 °C to 90 °C and the temperature was collected once every 3s. And the specific locations of thermocouples TC_1-TC_{13} are shown in Table 2.

2.2. Preparation of nanofluids

The working fluids used in the LHP were distilled water and CuO–H_2O nanofluids. The nanofluids were prepared by the two-step method: Mix the copper oxide nanoparticle, distilled water, and dispersants (SDBS), then use ultrasonic dispersion in water of

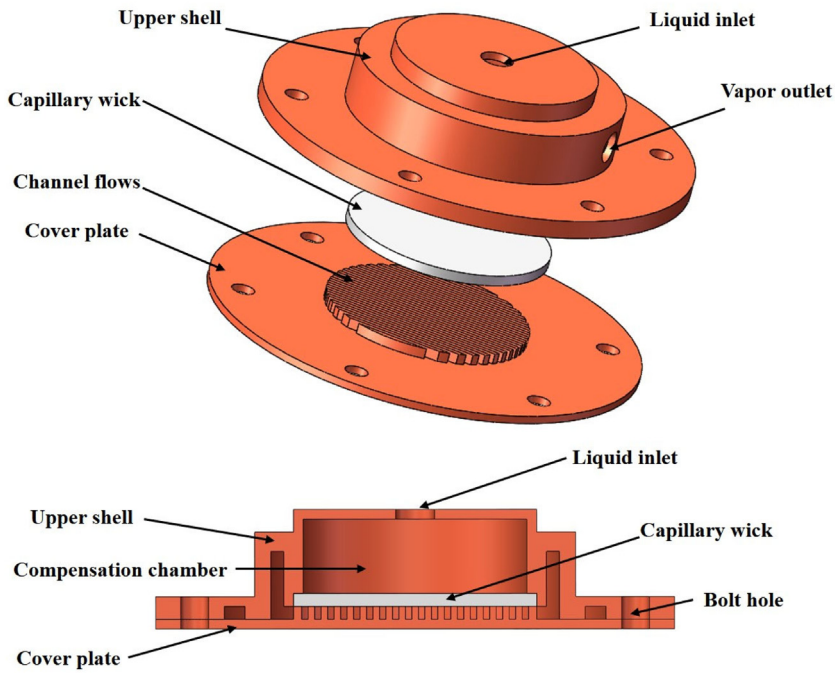

Fig. 1. The internal structure of the evaporator.

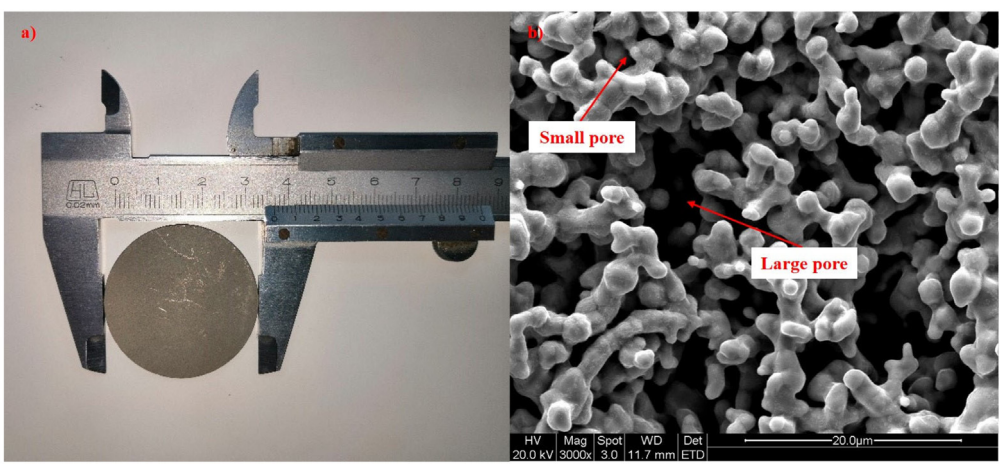

Fig. 2. Photographs of the biporous wick. (a) The appearance of the wick. (b) SEM photograph (3000-times) of a biporous wick for the same fabrication method.

40 °C for 8 h followed by magnetic stirring for 30 min to obtain CuO–H_2O nanofluids with the mass concentration of 0.5%.

The CuO nanoparticles were spherical copper oxide with an average diameter of 40 nanometers and their density was 0.79 g/cm^3. The photographic view of the CuO nanoparticles as seen by the naked eyes is shown in Fig. 4(a) and the SEM image is shown in Fig. 4(b).

The specific flow chart of preparation is shown in Fig. 5. The mass concentration of CuO particles in nanofluids is calculated by the followed equation:

$$\omega\% = \frac{M_{\mathrm{CuO}}}{M_{\mathrm{CuO}} + M_{base}} \times 100\% \tag{3}$$

where, M_{CuO} denotes the mass of nanoparticle (CuO) and M_{base} denotes the mass of base fluid.

2.3. Characteristics of nanofluids

Nanofluids can be considered stable if the mass concentration of solid particles no longer changes for a period, which shows that the nanofluids are no longer settling. The common evaluation methods for the stability of nanofluids include particle size distribution, gravity sedimentation observation, and Zeta potential analysis (Yu and Xie, 2012). The gravity sedimentation observation method is the simplest among them, which has been adopted in the present investigation.

Fig. 6 shows the variation of prepared 0.5 wt% CuO–H_2O nanofluids with time, and the right beaker was the control group without dispersants (SDBS), it is obvious that the nanoparticles in the control groups have fully settled in the second day, but the obvious settlement has not appeared in the experimental group that has dispersants. The nanofluids were still stable after a month which means the stability of the nanofluids were suitable for the working fluid in LHP.

Since the LHP system was made of copper, the contact angles of distilled water and CuO–H_2O nanofluid**s** were measured on a copper surface when the ambient temperature was 20 °C. To avoid rapid evaporation of small droplets on the surface, the image was selected within 20 s after the droplet contacted the

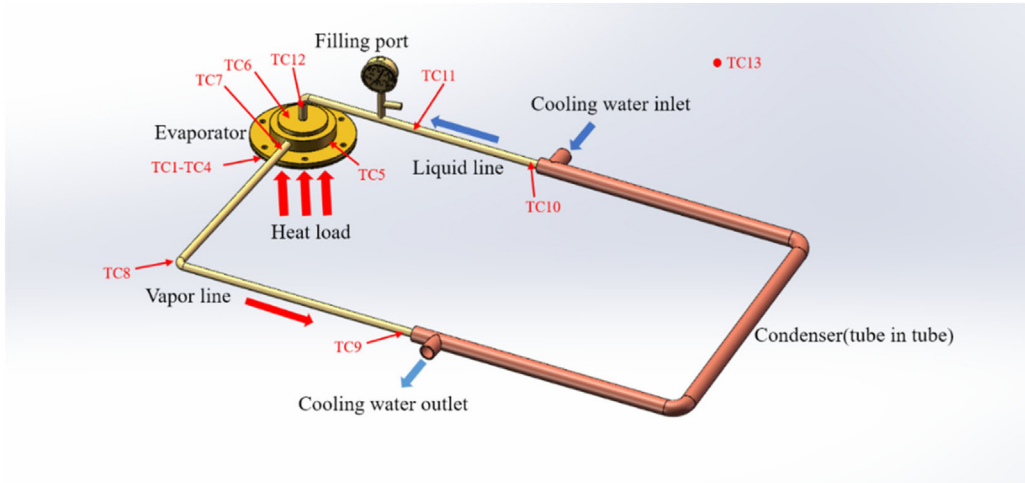

Fig. 3. The schematic diagram of the loop heat pipe.

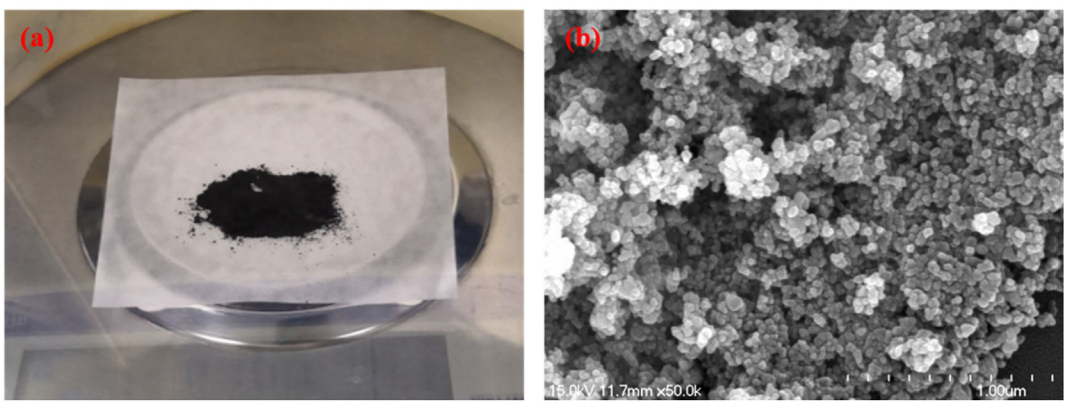

Fig. 4. (a) A photographic view of the CuO nanoparticles (b) The SEM image of CuO nanoparticles.

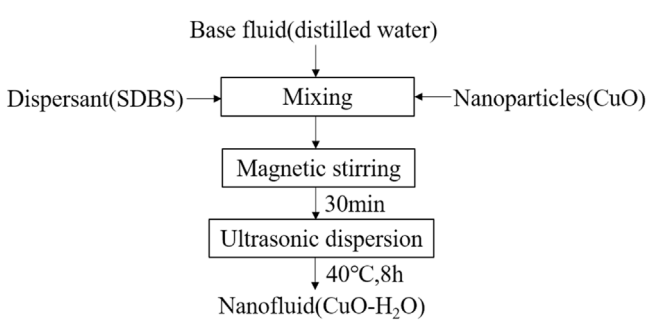

Fig. 5. The flow chart of preparation of CuO–H_2O nanofluids.

surface. The static contact angles of distilled water and CuO–H_2O nanofluids on a copper surface are shown in Fig. 7. The static contact angles of CuO–H_2O nanofluids were 65.35° and that of distilled water was 88.75°. The nanoparticles reduced the static contact angles by 26.36%. It can be seen that the nanofluid had a better wettability on the copper surface compared with distilled water.

3. Results

3.1. Thermal resistance analysis

Thermal resistance is often regarded as an important parameter of LHP to evaluate the thermal performance of LHP, which reflects the ability to remove heat from heat source. In the present work, the thermal resistances of the evaporator and the total system of the LHP have been calculated respectively. The thermal resistance of the LHP system reflects the thermal performance of the whole system, and the thermal resistance of the evaporator reflects the heat transfer effect between the heat source and the evaporator (Song et al., 2016).

The thermal resistance of the LHP system(R_{LHP}) is defined as:

$$R_{LHP} = \frac{T_{eva} - T_{cond}}{Q} \tag{4}$$

where, T_{eva} is the temperature of the evaporator wall, T_{cond} is the average temperature of the condenser which is the average inlet temperature and outlet temperature of the condenser, and Q is the heat load.

The thermal resistance of evaporator (R_{LHP})is defined as:

$$R_{eva} = \frac{T_{eva} - T_{eva_out}}{Q} \tag{5}$$

where, T_{eva} is the temperature of the evaporator wall, T_{eva_out} is the outlet temperature of the evaporator, and Q is the heat load.

The variation of R_{LHP} with heat load from 50 W to 290 W the sink temperature of 10 °C is shown in Fig. 8. R_{LHP} decreased with the increase of heat load and approaches a constant at high heat load in all cases, which included variable thermal resistance stage and constant thermal resistance stage. When the working fluid was distilled water, the value of R_{LHP} fluctuated from 0.795 °C/W at the heat load of 50 W to 0.394 °C/W at the heat load of 290 W

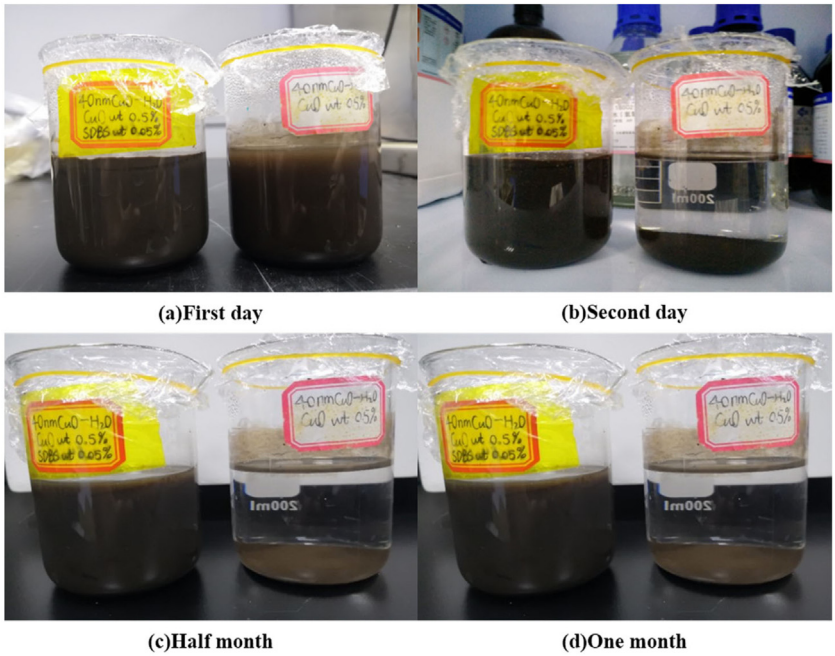

Fig. 6. Change of nanofluids with time (the beaker on the right was the control group without dispersant).

without dispersant).

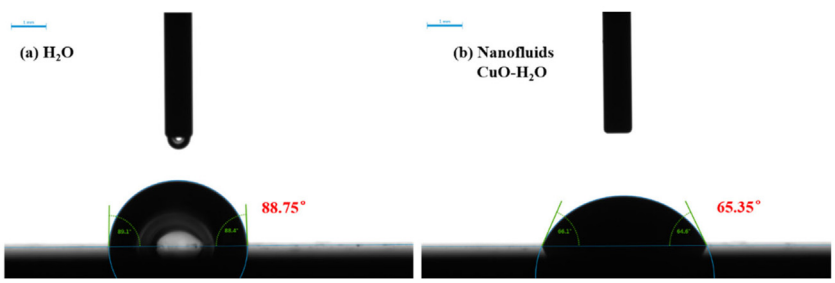

Fig. 7. (a) Static contact angle of distilled water on a copper surface (b) Static contact angle of CuO–H_2O nanofluids on a copper surface.

and the minimum of the value of R_{LHP} was 0.394 °C/W at the heat load of 290 W. When the working fluid were nanofluids, the value of R_{LHP} fluctuated from 0.655 °C/W at the heat load of 50 W to 0.372 °C/W at the heat load of 290 W and the minimum of the value of R_{LHP} was 0.372 °C/W at the heat load of 290 W. Using nanofluids as working fluid of LHP could reduce the thermal resistance of the system at the heat load of 50 W to 290 W. At the heat load of 50 W, the reduction was 17.6%, which was most significant compared with distilled water.

The variation of R_{eva} with heat load from 50 W to 290 W when the sink temperature was 10 °C is shown in Fig. 9. With distilled water employed as the working fluid, the heat resistance of the evaporator fluctuated within a range between 0.255 °C/W and 0.323 °C/W. The minimum heat resistance of the evaporator was 0.255 °C/W that occurred at a heat load of 50 W. With nanofluids as the working fluid, the heat resistance of the evaporator fluctuated between 0.212 °C/W and 0.255 °C/W. Similarly, the minimum heat resistance of the evaporator was 0.212 °C/W that occurred at a heat load of 50 W. Compared with distilled water working fluid, nanofluids working fluid could reduce the heat resistance of the evaporator. The maximum reduction ratio was 26.9% at a heat load of 50 W.

According to the thermal resistance results in the test, the nanofluids mainly contributed to decreasing the thermal resistance of the evaporator instead of that of the condenser. It could be inferred that nanofluids in the LHP mainly influence the evaporator and biporous wick. The nanoparticles in the biporous wick might increase the amount of vaporization at the evaporation surface so that the thermal resistance of the evaporator decreased.

The uncertainty of R_{LHP} can be calculated by

$$\frac{\delta R_{LHP}}{R_{LHP}} = \sqrt{(\frac{\delta y}{y})^2 + (\frac{\delta Q}{Q})^2} \tag{6}$$

$$\delta y = \sqrt{\sum_{i=1}^{4}(\frac{1}{4}\delta T_{eva,i})^2 + \sum_{i=1}^{2}(\frac{1}{2}\delta T_{c,i})^2} \tag{7}$$

$$y = T_{eva} - T_c \tag{8}$$

where $T_{eva,i}$ is the temperature at heater surface measured by four thermocouples and $T_{c,i}$ is the temperature at condenser inlet and outlet. Due to the accuracy of T-type thermocouples were ±0.5 °C, $\delta T_{eva,i}$ and $\delta T_{c,i}$ were all equal to 0.5 °C. The accuracy of the power meter was 0.5%. Thus, the uncertainty of R_{LHP} was ± 2.7% at low heat load (Q = 50 W) and ± 0.83% at high heat load (Q = 290 W). Similarly, the uncertainty of R_{eva} was ± 6.67% at low heat load (Q = 50 W) and ± 0.11% at high heat load (Q = 290 W)

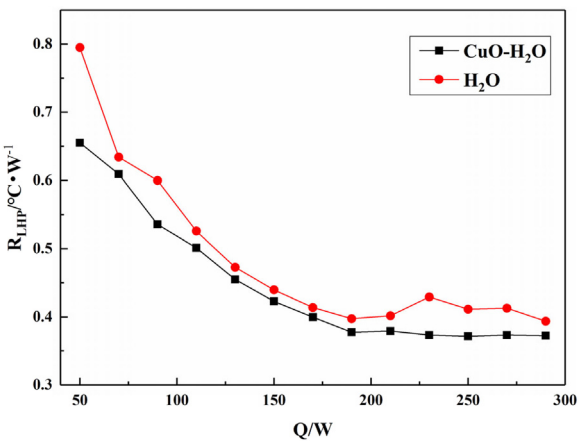

Fig. 8. Change of R_{LHP} with heat load.

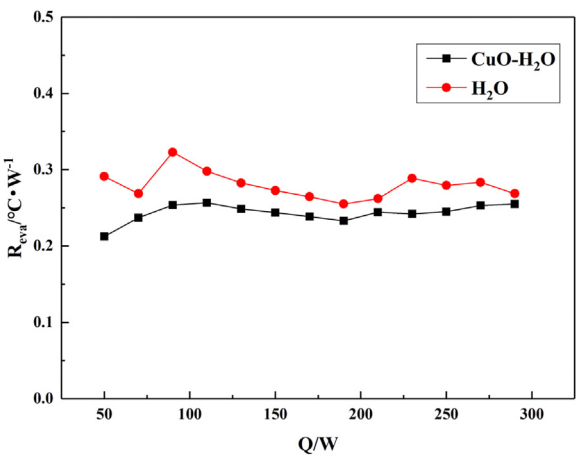

Fig. 9. Change of R_{eva} with heat load.

3.2. Startup tests

The startup process is one of the most important operating characteristics to evaluate the reliability and stability of an LHP at fixed heat load. Fig. 10 shows the star-tup process of LHP at the heat load of 20 W and the working fluid was distilled water, which was a typical failure of the setup process of low heat load. After applying heat load, evaporator temperature rose gradually within 10 min and the inlet temperature of the condenser increased sharply, indicating that the working fluid in the evaporator vaporized and entered the condenser. Then the temperature rose slowly within 1 h and the inlet temperature of the condenser decreased within 40 min since the heat load was so low that the rate of evaporation was lower than that of condensation and the supercooled liquid returned into the evaporator. The evaporator temperature kept rising and the circulation of working fluid in LHP failed.

At the same heat load of 20 W, the temperature variation of LHP with nanofluids is shown in Fig. 11. Compared with distilled water, the LHP started successfully in nearly 40 min and temperature fluctuation appeared in the case. The rate of evaporation was still lower than of condensation rate but better than that of distilled water. It is attributed to the temperature fluctuation of LHP after startup. The inlet temperature of the condenser fluctuated was not synchronized with the outlet temperature of the evaporator, indicating that the vapor–liquid interface might move near the inlet of the condenser since the rate difference of

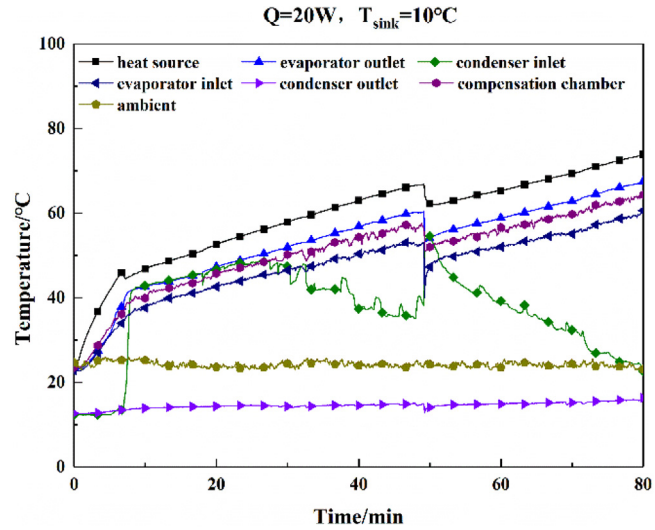

Fig. 10. Startup at 20 W-10 °C-Distilled water.

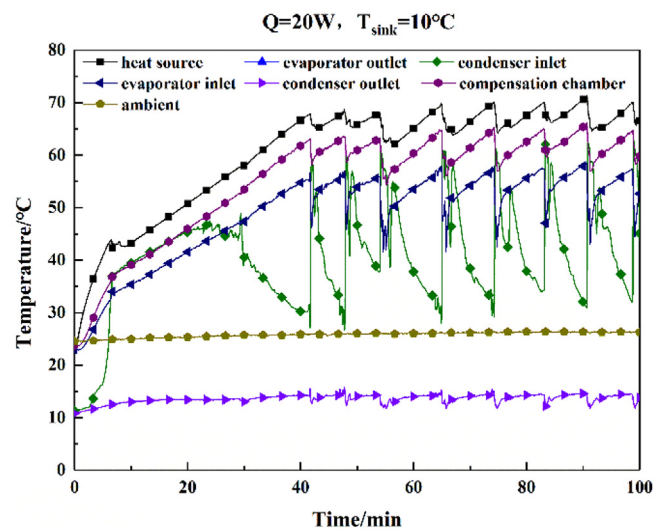

Fig. 11. Startup at 20 W-10 °C-Nanofluids.

condensation and evaporation. The startup performance of LHP with nanofluids was better than that of water as the working fluid at the low heat load of 20 W.

Fig. 12 shows the process of the successful startup of LHP with distilled water as working fluid and the heat load was 40 W. Similar to distilled water, the temperature of the evaporator and the inlet temperature of the condenser rose gradually after applying heat load, then the temperature of the evaporator suddenly dropped and continued to rise. Finally, temperature fluctuations appeared in the 30 min whose amplitude was about 5 °C and period was about 10 min. It could be concluded the minimum startup heat load with distilled water as working fluid was 40 W while that of nanofluids was 20 W in the LHP system.

Figs. 13 and 14 show the stable startup process of LHP with distilled water and nanofluids, respectively. With higher heat load, the fluctuation of temperature was smaller. The fluctuation of the inlet temperature evaporator was still obvious. The inlet located above the compensation chamber evaporator made the vapor generated from the compensation chamber easier to enter the inlet of the evaporator due to backward thermal conductivity. With water as the working fluid, LHP could startup smoothly

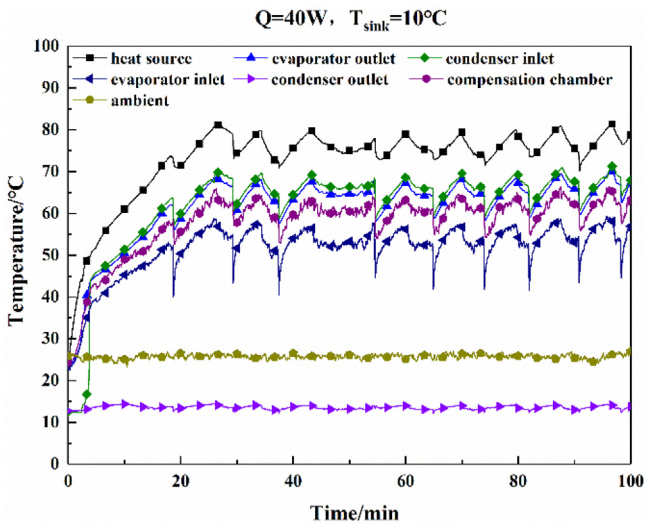

Fig. 12. Startup at 40 W-10 °C-Distilled water.

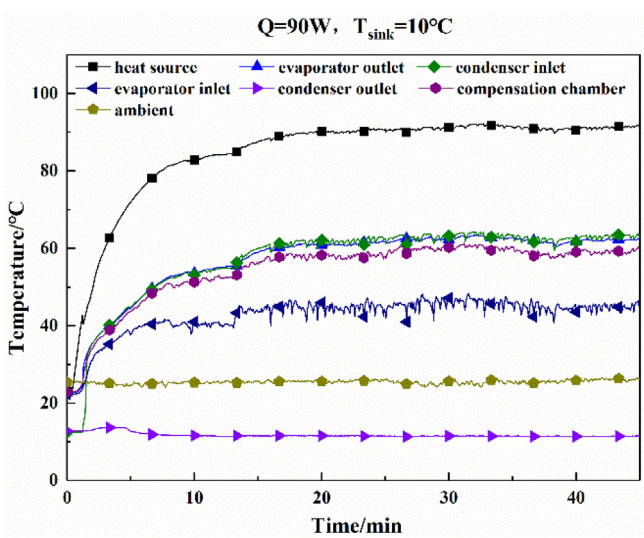

Fig. 13. Startup at 90 W-10 °C-Distilled water.

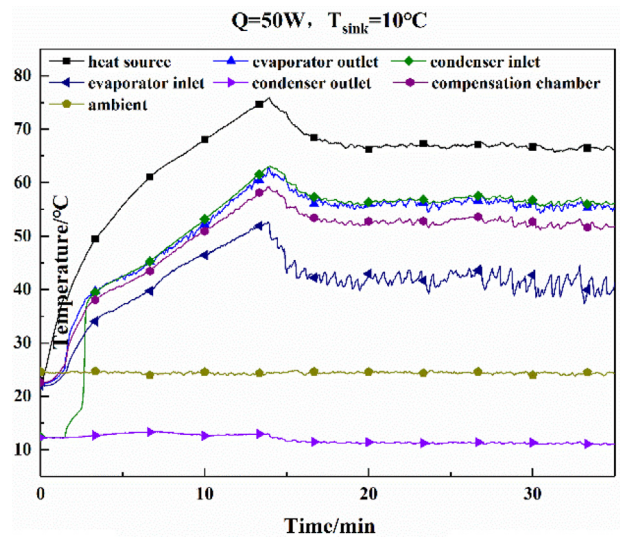

Fig. 14. Startup at 50 W-10 °C-Nanofluids.

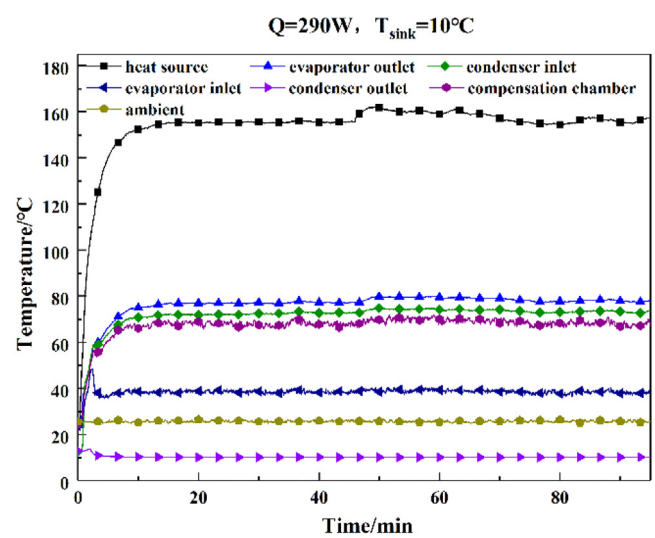

Fig. 15. Startup at 290 W-10 °C-Distilled water.

without temperature fluctuation at the heat load of minimum thermal load 90 W. With nanofluids as working fluid, the smooth startup minimum heat load could be reduced to 50 W.

Figs. 15 and 16 show the startup process at the heat load of 290 W with distilled water and nanofluids. With distilled water as the working fluid, the average outlet temperature of the evaporator was 77.9 °C and the temperature of the evaporator wall was 155.8 °C within 5 min after the LHP entered a stable state, but the maximum outlet temperature reached 80 °C in the stage of fluctuation. Compared with distilled water, the inlet temperature of the evaporator was reduced to 74.7 °C which lowered 3 °C and the temperature of the evaporator wall was 148.7 °C which lowered 8 °C with nanofluids at the same heat load. On the premise that the outlet temperature of the evaporator did not exceed 80 °C, it could be considered that the maximum heat load of the LHP system with distilled water was 290 W while that of nanofluids increased to 310 W which is shown in Fig. 17. Wan et al. used Cu–water nanofluids as working fluid in a miniature loop heat pipe and the nanofluids were composed of distilled water and Cu nanoparticles. A sintered red copper powder sheet with a porosity of 53% was used as a porous wick and the area of the copper heater was 27.5 cm^2 and the range of heat load was 25–100 W so that heat flux ranged from 0.9 to 3.6 W/cm^2. In this work, the heat flux ranged from 5 to 29 W/cm^2 in operation. Compared with the study Ref. Wan et al. (2015) the capillary biporous wick showed better thermal performance than the traditional sintered wick.

The temperature variation of the evaporator wall at different heat loads within the range of 50 W to 190 W is shown in Fig. 18. Compared with distilled water, the temperature of the evaporator wall decreased significantly by 12.7 °C at 50 W. From 110 W to 170 W, there was no obvious difference between these two working fluids. From 190 W to 290 W, the temperature of the evaporator wall decreased by 13.5 °C significantly at 230 W.

3.3. System response to variable heat load

The operation of the variable heat load is also an important characteristic, reflecting the stability of LHP under variable operating conditions. The operation of variable heat load in this experiment starts from a certain heat load within the normal startup range of LHP. After starting successfully, the heat load was

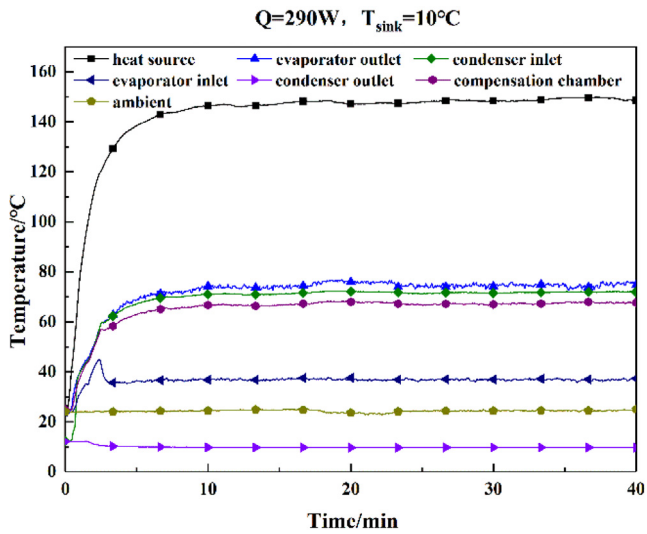

Fig. 16. Startup at 290 W-10 °C-Nanofluids.

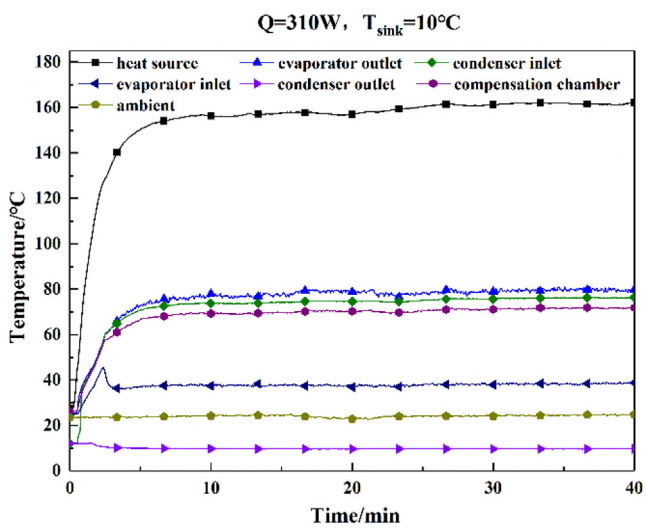

Fig. 17. Startup at 310 W-10 °C-Nanofluids.

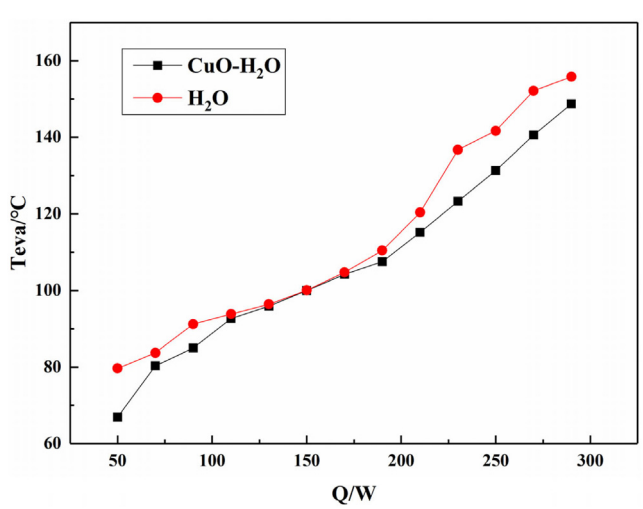

Fig. 18. The temperature of the evaporator wall.

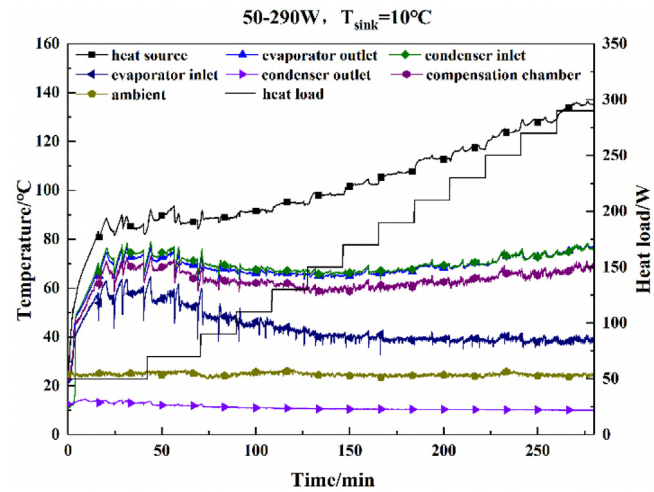

Fig. 19. The temperature response to variable heat load from 50 W to 290 W-10 °C-Distilled water.

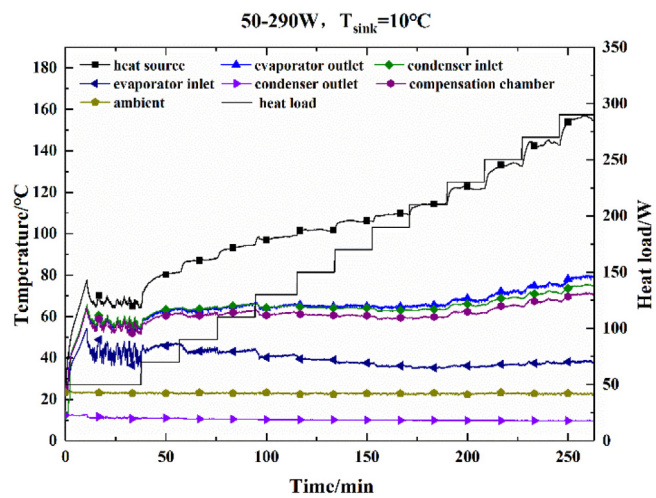

Fig. 20. The temperature response to variable heat load from 50 W to 290 W-10 °C-Nanofluids.

increased by 20 W, and the duration of each heat load was 20 min or 30 min.

Figs. 19 and 20 show the temperature change of LHP at variable heat load when distilled water and nanofluids were used as working fluids, respectively. The temperature fluctuation was obvious when the heat load was between 50 W and 90 W. The heat load was so low that the evaporation rate in the evaporator was less than the condensation rate in the condenser. The pressure of LHP was not stable, which made the vapor–liquid interface enter the condenser and return into the liquid line repeatedly, causing temperature fluctuation. At the heat load from 90 W to 290 W, the temperature tended to be stable within a short time without obvious fluctuation after changing the heat load. Compared with distilled water as the working fluid, the response speed was faster at a high heat load with nanofluids. With heat load increased gradually, the flow of the working fluid would increase as well which caused the backflow velocity of condensed liquid into the evaporator faster. Therefore, the temperature of the evaporator inlet appeared to lower with the heat load increasing. The same phenomenon could be found in previous researches on variable heat load tests in Ref. Zhang et al. (2021, 2020).

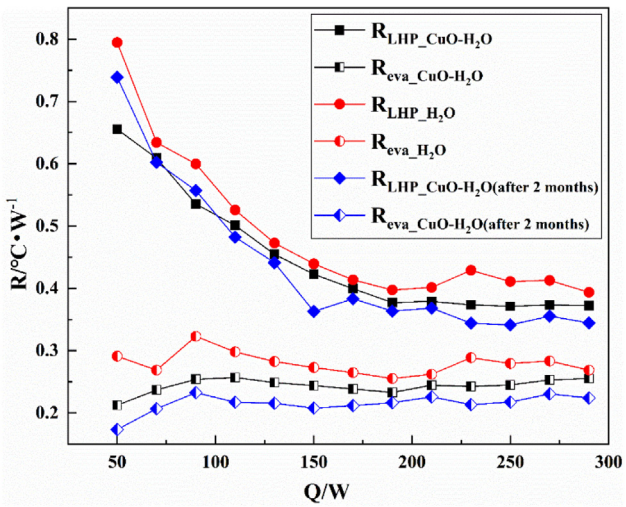

Fig. 21. Change of R_{eva} and R_{LHP} with heat load.

3.4. Performance degradation tests

Whether the benefit of nanofluids used in LHP can be still effective after some time has been a concern since the steady-state of nanofluids is unknown in the LHP system. If the settlement of nanofluids has appeared, the effects of the nanofluids may decrease or even influence the normal operation of the LHP system. To realize the problem, the performance degradation tests were conducted after 2 months. At the period of 2 months, the LHP system was out of work and the repeated tests were conducted under the same condition.

Fig. 21 shows the change of R_{eva} and R_{LHP} with heat load from 50 W to 290 W in the case of distilled water as working fluid, nanofluids (CuO–H_2O) as working fluid, and the case after 2 months. Compared with the former experiment, the heat resistance of the evaporator was 0.173 °C/W and the heat resistance of the LHP system was 0.739 °C/W at 50 W when the working fluid were nanofluids (CuO–H_2O) after 2 months, which was lower 11.4% than before. The LHP with nanofluids as working fluid still operated normally and the change of thermal resistance with the varies of heat load had the same tendency as the previous experiment. Even at certain heat loads, the thermal resistances of evaporator and LHP system with nanofluids as working fluid were reduced more. Therefore, using nanofluids (CuO–H_2O) in the LHP system with sintered capillary wick could benefit the heat transfer performance and keep steady within a length of time.

4. Conclusion

CuO–H_2O nanofluids with a mass fraction of 0.5%wt were used in a flat evaporator with a nickel powder sintered capillary biporous wick for the first time in this experiment. When the sink temperature was 10 °C, the thermal performance of startup at fixed heat load, system response to variable heat load, and performance degradation were tested with nanofluids and distilled water. The conclusions could be drawn as follows from the experimental results:

(1) An LHP with a flat evaporator was designed and nanofluids were used in the nickel powders sintered capillary wick for the first time. Using nanofluids in LHP with sintered capillary wick could benefit the heat transfer performance and the nanoparticles would not settle to clog the sintered capillary wick and the operation of LHP kept steady within 2 months in performance degradation tests.

(2) In the test of the startup of LHP, under the premise of outlet temperature no more than 80 °C, the heat load range of successful startup increased from 40 W–290 W to 20 W–310 W with nanofluids as working fluid. The thermal resistances of the evaporator and system were reduced and the effect was most significant at a heat load of 50 W. The temperature of the evaporator wall was reduced by 12.7 °C, the thermal resistance of the evaporator was reduced by 26.9% and the thermal resistance of the LHP system was reduced by 17.6%.

(3) Compared with distilled water, the speed of response to the variable heat load of the LHP became faster with nanofluids as working fluid. And the temperature fluctuation was smaller than that of distilled water.

CRediT authorship contribution statement

Tianyuan Zhao: Conceptualization, Methodology, Software, Validation, Formal analysis, Investigation, Data curation, Writing – original draft, Writing – review & editing, Visualization. **Zhengyuan Ma:** Methodology, Software, Validation, Data curation. **Zikang Zhang:** Methodology, Software, Data curation. **Weizhong Deng:** Methodology, Software. **Rui Long:** Conceptualization, Resources, Supervision, Project administration. **Wei Liu:** Resources, Supervision, Project administration, Funding acquisition. **Lei Ma:** Conceptualization, Resources, Project administration. **Zhichun Liu:** Conceptualization, Resources, Supervision, Project administration, Funding acquisition.

Declaration of competing interest

The authors declare that they have no known competing financial interests or personal relationships that could have appeared to influence the work reported in this paper.

Acknowledgments

The work was supported by the National Natural Science Foundation of China (Nos. 51776079 & 52076088) and the Open Research Fund of Key Laboratory of Space Utilization, Chinese Academy of Sciences (No. LSU-KFJJ-2019-07).

References

Alawi, O.A., Sidik, N.A.C., Mohammed, H.A., Syahrullail, S., 2014. Fluid flow and heat transfer characteristics of nanofluids in heat pipes: A review. Int. Commun. Heat Mass Transfer 56, 50–62. http://dx.doi.org/10.1016/j.icheatmasstransfer.2014.04.014.

Chen, B.B., Liu, W., Liu, Z.C., Li, H., Yang, J.G., 2012. Experimental investigation of loop heat pipe with flat evaporator using biporous wick. Appl. Therm. Eng. 42, 34–40. http://dx.doi.org/10.1016/j.applthermaleng.2012.03.006.

Choi, S.U.S., 1995. Enhancing thermal conductivity of fluids with nanoparticles. Am. Soc. Mech. Eng. Fluids Eng. Div. FED 231, 99–105.

Choi, S.U.S., Li, S., Eastman, J.A., 1999. Measuring thermal conductivity of fluids containing oxide nanoparticles. J. Heat Transfer 121, 280–289. http://dx.doi.org/10.1115/1.2825978.

Gupta, N.K., Tiwari, A.K., Ghosh, S.K., 2018. Heat transfer mechanisms in heat pipes using nanofluids – A review. Exp. Therm. Fluid Sci. 90, 84–100. http://dx.doi.org/10.1016/j.expthermflusci.2017.08.013.

Gürü, M., Sözen, A., Karakaya, U., Çiftçi, E., 2019. Influences of bentonite-deionized water nanofluid utilization at different concentrations on heat pipe performance: An experimental study. Appl. Therm. Eng. 148, 632–640. http://dx.doi.org/10.1016/j.applthermaleng.2018.11.024.

He, S., Zhao, J., Liu, Z. chun, Tian, W., Yang, J. guo, Liu, W., 2018. Experimental investigation of loop heat pipe with a large squared evaporator for cooling electronics. Appl. Therm. Eng. 144, 383–391. http://dx.doi.org/10.1016/j.applthermaleng.2018.08.075.

Ji, X., Wang, Y., Xu, J., Huang, Y., 2017. Experimental study of heat transfer and start-up of loop heat pipe with multiscale porous wicks. Appl. Therm. Eng. 117, 782–798. http://dx.doi.org/10.1016/j.applthermaleng.2017.01.084.

Ku, J., 2007. Operating Characteristics of Loop Heat Pipes - NASA.Pdf.

Li, H., Liu, Z.C., Chen, B. Bin, Liu, W., Li, C., Yang, J., 2012. Development of biporous wicks for flat-plate loop heat pipe. Exp. Therm. Fluid Sci. 37, 91–97. http://dx.doi.org/10.1016/j.expthermflusci.2011.10.007.

Li, Y., Lv, L.C., Liu, Z.H., 2010. Influence of nanofluids on the operation characteristics of small capillary pumped loop. Energy Convers. Manage. 51, 2312–2320. http://dx.doi.org/10.1016/j.enconman.2010.04.004.

Liu, Z.H., Li, Y.Y., 2012. A new frontier of nanofluid research - Application of nanofluids in heat pipes. Int. J. Heat Mass Transfer 55, 6786–6797. http://dx.doi.org/10.1016/j.ijheatmasstransfer.2012.06.086.

Liu, Z.C., Liu, W., Nakayama, A., 2007. Flow and heat transfer analysis in porous wick of CPL evaporator based on field synergy principle. Heat Mass Transfer Stoffuebertrag. 43, 1273–1281. http://dx.doi.org/10.1007/s00231-006-0213-8.

Martin, K., Sözen, A., Çiftçi, E., Ali, H.M., 2020. An experimental investigation on aqueous Fe–CuO hybrid nanofluid usage in a plain heat pipe. Int. J. Thermophys. 41, 1–21. http://dx.doi.org/10.1007/s10765-020-02716-6.

Maydanik, Y.F., 2005. Loop heat pipes. Appl. Therm. Eng. 25, 635–657. http://dx.doi.org/10.1016/j.applthermaleng.2004.07.010.

Nakamura, K., Odagiri, K., Nagano, H., 2016. Study on a loop heat pipe for a long-distance heat transport under anti-gravity condition. Appl. Therm. Eng. 107, 167–174. http://dx.doi.org/10.1016/j.applthermaleng.2016.06.162.

Putra, N., Saleh, R., Septiadi, W.N., Okta, A., Hamid, Z., 2014. Thermal performance of biomaterial wick loop heat pipes with water-base Al2O3 nanofluids. Int. J. Therm. Sci. 76, 128–136. http://dx.doi.org/10.1016/j.ijthermalsci.2013.08.020.

Riehl, R.R., Santos, N. Dos, 2012. Water-copper nanofluid application in an open loop pulsating heat pipe. Appl. Therm. Eng. 42, 6–10. http://dx.doi.org/10.1016/j.applthermaleng.2011.01.017.

Sadeghinezhad, E., Mehrali, Mohammad, Rosen, M.A., Akhiani, A.R., Tahan Latibari, S., Mehrali, Mehdi, Metselaar, H.S.C., 2016. Experimental investigation of the effect of graphene nanofluids on heat pipe thermal performance. Appl. Therm. Eng. 100, 775–787. http://dx.doi.org/10.1016/j.applthermaleng.2016.02.071.

Semenic, T., Lin, Y.Y., Catton, I., Sarraf, D.B., 2008. Use of biporous wicks to remove high heat fluxes. Appl. Therm. Eng. 28, 278–283. http://dx.doi.org/10.1016/j.applthermaleng.2006.02.030.

Singh, R., Akbarzadeh, A., Mochizuki, M., 2008. Operational characteristics of a miniature loop heat pipe with flat evaporator. Int. J. Therm. Sci. 47, 1504–1515. http://dx.doi.org/10.1016/j.ijthermalsci.2007.12.013.

Song, H., Zhi-chun, L., Jing, Z., Chi, J., Jin-guo, Y., Wei, L., 2016. Experimental study of an ammonia loop heat pipe with a flat plate evaporator. Int. J. Heat Mass Transfer 102, 1050–1055. http://dx.doi.org/10.1016/j.ijheatmasstransfer.2016.07.014.

Sözen, A., Ciftçi, E., Keçel, S., Gürü, M., Variyenli, H.İ., Karakaya, U., 2018a. Usage of a diatomite-containing nanofluid as the working fluid in a wickless loop heat pipe: Experimental and numerical study. Heat Transfer Res. 49, 1721–1744. http://dx.doi.org/10.1615/HeatTransRes.2018025111.

Sözen, A., Gürü, M., Khanlari, A., Çiftçi, E., 2019. Experimental and numerical study on enhancement of heat transfer characteristics of a heat pipe utilizing aqueous clinoptilolite nanofluid. Appl. Therm. Eng. 160, 114001. http://dx.doi.org/10.1016/j.applthermaleng.2019.114001.

Sözen, A., Gürü, M., Menlik, T., Karakaya, U., Çiftçi, E., 2018b. Experimental comparison of triton X-100 and sodium dodecyl benzene sulfonate surfactants on thermal performance of TiO2–deionized water nanofluid in a thermosiphon. Exp. Heat Transfer 31, 450–469. http://dx.doi.org/10.1080/08916152.2018.1445673.

Tharayil, T., Asirvatham, L.G., Dau, M.J., Wongwises, S., 2017. Entropy generation analysis of a miniature loop heat pipe with graphene–water nanofluid: Thermodynamics model and experimental study. Int. J. Heat Mass Transfer 106, 407–421. http://dx.doi.org/10.1016/j.ijheatmasstransfer.2016.08.035.

Tharayil, T., Asirvatham, L.G., Ravindran, V., Wongwises, S., 2016. Thermal performance of miniature loop heat pipe with graphene-water nanofluid. Int. J. Heat Mass Transfer 93, 957–968. http://dx.doi.org/10.1016/j.ijheatmasstransfer.2015.11.011.

Tsai, C.Y., Chien, H.T., Ding, P.P., Chan, B., Luh, T.Y., Chen, P.H., 2004. Effect of structural character of gold nanoparticles in nanofluid on heat pipe thermal performance. Mater. Lett. 58, 1461–1465. http://dx.doi.org/10.1016/j.matlet.2003.10.009.

Wan, Z., Deng, J., Li, B., Xu, Y., Wang, X., Tang, Y., 2015. Thermal performance of a miniature loop heat pipe using water-copper nanofluid. Appl. Therm. Eng. 78, 712–719. http://dx.doi.org/10.1016/j.applthermaleng.2014.11.010.

Wang, D., Liu, Z., Shen, J., Jiang, C., Chen, B., Yang, J., Tu, Z., Liu, W., 2014. Experimental study of the loop heat pipe with a flat disk-shaped evaporator. Exp. Therm. Fluid Sci. 57, 157–164. http://dx.doi.org/10.1016/j.expthermflusci.2014.04.017.

Wang, G.S., Song, B., Liu, Z.H., 2010. Operation characteristics of cylindrical miniature grooved heat pipe using aqueous CuO nanofluids. Exp. Therm. Fluid Sci. 34, 1415–1421. http://dx.doi.org/10.1016/j.expthermflusci.2010.07.004.

Yeh, C.C., Chen, C.N., Chen, Y.M., 2009. Heat transfer analysis of a loop heat pipe with biporous wicks. Int. J. Heat Mass Transfer 52, 4426–4434. http://dx.doi.org/10.1016/j.ijheatmasstransfer.2009.03.059.

Yılmaz Aydın, D., Çiftçi, E., Gürü, M., Sözen, A., 2021b. The impacts of nanoparticle concentration and surfactant type on thermal performance of a thermosyphon heat pipe working with bauxite nanofluid. Energy Sources A 43, 1524–1548. http://dx.doi.org/10.1080/15567036.2020.1800141.

Yilmaz Aydin, D., Gürü, M., Sözen, A., Çiftçi, E., 2021a. Investigation of the effects of base fluid type of the nanofluid on heat pipe performance. Proc. Inst. Mech. Eng. A 235, 124–138. http://dx.doi.org/10.1177/0957650920916285.

Yu, W., Xie, H., 2012. A review on nanofluids: Preparation, stability mechanisms, and applications. J. Nanomater. 2012, http://dx.doi.org/10.1155/2012/435873.

Zaaroura, I., Harmand, S., Carlier, J., Toubal, M., Fasquelle, A., Nongaillard, B., 2021. Thermal performance of self-rewetting gold nanofluids: Application to two-phase heat transfer devices. Int. J. Heat Mass Transfer 174, 121322. http://dx.doi.org/10.1016/j.ijheatmasstransfer.2021.121322.

Zhang, Z., Zhang, H., Ma, Z., Liu, Z., Liu, W., 2020. Experimental study of heat transfer capacity for loop heat pipe with flat disk evaporator. Appl. Therm. Eng. 173, 115183. http://dx.doi.org/10.1016/j.applthermaleng.2020.115183.

Zhang, Z., Zhao, R., Liu, Z., Liu, W., 2021. Application of biporous wick in flat-plate loop heat pipe with long heat transfer distance. Appl. Therm. Eng. 184, 116283. http://dx.doi.org/10.1016/j.applthermaleng.2020.116283.

Zhao, R., Zhang, Z., Zhao, S., Cui, H., Liu, Z., Liu, W., 2021. Experimental study of flat-disk loop heat pipe with R1233zd(E) for cooling terrestrial electronics. Appl. Therm. Eng. 197, 117385. http://dx.doi.org/10.1016/j.applthermaleng.2021.117385.

Zhou, R., Fu, S., Li, H., Yuan, D., Tang, B., Zhou, G., 2019. Experimental study on thermal performance of copper nanofluids in a miniature heat pipe fabricated by wire electrical discharge machining. Appl. Therm. Eng. 160, 113989. http://dx.doi.org/10.1016/j.applthermaleng.2019.113989.